



Structural relationships in and around the Rheasilvia basin on Vesta

Hiu Ching Jupiter Cheng^{*}, Christian Klimczak

Center for Planetary Tectonics, Department of Geology, University of Georgia, Athens, GA, 30602, USA



ABSTRACT

The Rheasilvia basin is an impact structure occupying most of Vesta's southern hemisphere. Divalia Fossae, a set of circum-equatorial troughs, were previously proposed to be concentric around the basin, which is widely regarded as evidence that the Rheasilvia impact directly caused the formation of the troughs. Here, we produce a structural map of Rheasilvia that allows for geologic interpretations and quantitative analyses of structure orientations and densities. We mapped basin-bounding scarps, scarps within the basin, ridges, and undefined lineaments. Scarps abound near the basin rim, with ridges being densely located on the basin floor near the central mound, forming a spiral pattern. This pattern is well-preserved on the basin floor except in the area superposing the older Veneneia basin, indicating that pre-existing Veneneia structures substantially influenced those of Rheasilvia. This implies that the lithosphere must have remained highly shattered after the Veneneia impact until Rheasilvia was emplaced. The Divalia Fossae cross-cut the Rheasilvia basin, and reanalysis of the geometric relationship between both landforms reveals that the troughs are not concentric around the basin center. These results are inconsistent with the previous hypothesis of trough formation and require a reconsideration of Vesta's tectonic history.

1. Introduction

1.1. Geology of the Rheasilvia Basin

The existence of a major impact basin on Asteroid 4 Vesta, hereon referred to as Vesta, was first hypothesized when Hubble Space Telescope observations revealed a large depression in the south polar region of the asteroid (Thomas et al., 1997). The Dawn mission to Vesta (Russell and Raymond, 2011) revealed that the basin is 450 km in diameter, which is ~85% of the mean diameter of the asteroid, and that it occupies a large portion of the southern hemisphere. The impact that formed the basin is thought to be the youngest global-scale impact on Vesta (Schenk et al., 2012), and it likely excavated sufficient crustal material to have created the Vestoid asteroid family (Marzari et al., 1996; Asphaug, 1997) and the howardite-eucrite-diogenite (HED) meteorites (McCord et al., 1970; Drake and Consolmagno, 1977).

The Framing Camera (FC; Sierks et al., 2011) aboard the Dawn spacecraft captured high-resolution images of the Rheasilvia basin (Roatsch et al., 2015), allowing the construction of a detailed digital terrain model (DTM; Fig. 1; Preusker et al., 2016). The Rheasilvia basin is roughly hexagonal and outlined by discontinuous scarps (Fig. 1; Schenk et al., 2012), with the most prominent one named Matronalia Rupes (Fig. 1). No large melt sheet associated with the impact is observed, and its absence is interpreted to indicate a slow impactor (O'Brien and Sykes, 2011). Spacecraft observations also revealed a second large basin, Veneneia, that is partly superposed by the Rheasilvia

basin. Veneneia is inferred to have a diameter of ~421 km (Fig. 1; Jaumann et al., 2012; Marchi et al., 2012; Schenk et al., 2012). The basin rim of Rheasilvia that superposes the Veneneia depression has a lower elevation when compared with those portions of the rim that fall outside this depression (Fig. 1). This asymmetry was previously interpreted to be caused either by the pre-existing Veneneia topography (Collins et al., 2008) or by an oblique impact (Poelchau and Kenkmann, 2008).

Yingst et al. (2014) mapped terrains and structures of the Rheasilvia basin as part of the geological mapping effort of Vesta. The basin has a large central mound, a broad sloping basin floor with ridge-and-groove terrain, and mass-wasting materials. The irregular central mound (Fig. 1) is bisected by structures aligned with the larger structural trend of the basin floor. The basin floor has curvilinear ridges, grooves, and inward-facing scarps of kilometers to tens of kilometers long and a few kilometers high. These structures form two pronounced trends with one sub-radial from the mound and another parallel to basin-bounding scarps, generating a pervasive spiral pattern within the basin floor (Fig. 1; Schenk et al., 2012; Yingst et al., 2014). The spiral pattern was previously described as clockwise when measured from the basin center towards the rims (e.g., Schenk et al., 2012; 2022).

Numerical modeling (Jutzi et al., 2013) and the prediction of mass motion related to the Rheasilvia impact on a fast-spinning asteroid (Otto et al., 2016) support the hypothesis that these structures are remnants of mass wasting that occurred during the original modification with their orientations influenced by the Coriolis effect (Schenk et al., 2012; Otto et al., 2013; Jutzi et al., 2013). The observed spiral pattern is consistent

* Corresponding author.

E-mail address: jupiterchc@uga.edu (H.C.J. Cheng).

with the prediction that deflections of materials moving from the basin rim towards the south pole during the modification stage, in which the horizontal component of the Coriolis effect should be to the left in the southern hemisphere under the rotational direction of Vesta (i.e., rotating counterclockwise as viewed from above the north pole). Mass-wasting materials were deposited along the bases of steep slopes and basin-bounding scarps, indicating the mobility of the regolith (Jaumann et al., 2012; Pieters et al., 2012). Several types of mass-wasting structures are identified within the Rheasilvia basin, including flow-like patterns, creep-like mounds (which are elongated positive-relief landforms with a straight or slightly curved shape), rotational slumping, landslides, and curved ridges (Otto et al., 2013).

Despite its large size, the geomorphology of the Rheasilvia basin is unlike those of large multi-ring impact structures on other terrestrial bodies, such as the Moon or Mercury (Melosh, 1989), but it is like large

(complex) craters on low-gravity bodies with deep depressions and broad central mounds (Schenk et al., 2012). The spiral deformation pattern within the Rheasilvia basin is unique among large impact structures throughout the solar system in its size and preservation. Although these structures have been mapped at a large scale or locally in multiple works (e.g., Otto et al., 2013; Krohn et al., 2014; Yingst et al., 2014), a detailed structural map has not been constructed for the entire basin using a set of clearly defined and consistently applied mapping criteria. The basin is outlined by stratigraphic units in the geologic map from Yingst et al. (2014), but the rim and its center have yet to be defined by structural mapping and geometric analysis.

1.2. Basin relationship with Divalia Fossae

Dawn images also revealed the presence of two sets of large-scale

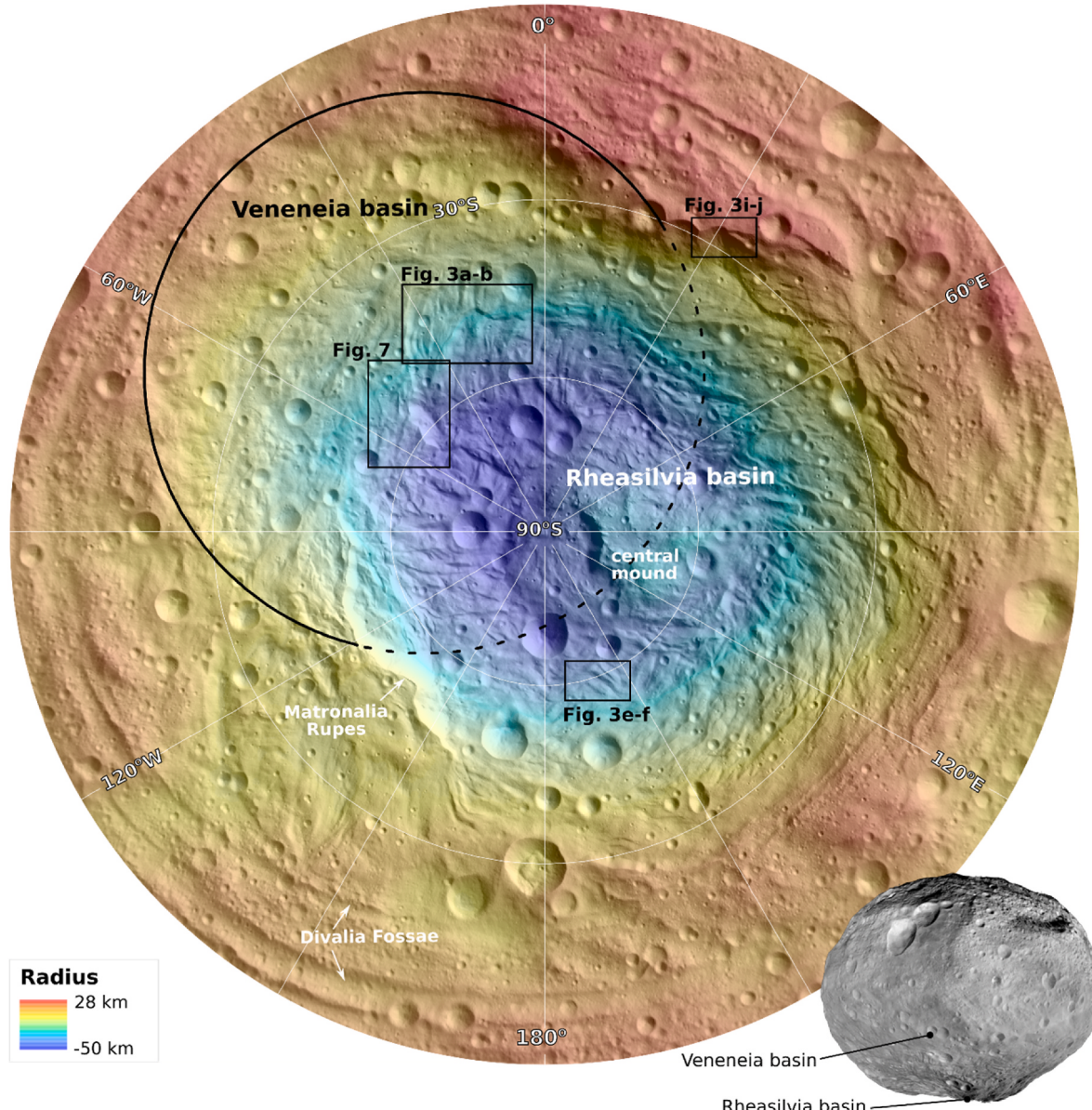


Fig. 1. Overview map of the Rheasilvia and Veneneia basins displayed as hillshade generated from the Dawn Digital Terrain Model (DTM; Preusker et al., 2016) with the solar azimuth of 56°E and incidence angle of 45°, color-coded by elevation in south polar stereographic projection. The reference elevation is defined to be the mean planetary radius of 262 km. The estimated circular basin rim of Veneneia basin is outlined with the preserved part as a black solid line and the part superposed by the Rheasilvia basin as a black dotted line. The location of the Divalia Fossae, the Rheasilvia central mound, and Matronalia Rupes are also indicated. For global reference, a Framing Camera image of Vesta is displayed at the lower right with the Veneneia and Rheasilvia basins labeled at the southern hemisphere. (For interpretation of the references to color in this figure legend, the reader is referred to the Web version of this article.)

troughs named Divalia and Saturnalia Fossae. The Divalia Fossae encircle about two-thirds of the asteroid at the equator, and their width ranges from several 100s of meters to 20.5 km. The Saturnalia Fossae are oriented northwest–southeast, and differ in orientation from the Divalia Fossae by approximately 30°. They are exposed only in the northern hemisphere, and their southern extent is truncated by the Divalia Fossae. The poles of planes defined along the Divalia and Saturnalia Fossae cluster near the centers of Rheasilvia and Veneneia impact basins, respectively, which is widely regarded as a genetic link between the troughs and basins (Jaumann et al., 2012; Scully et al., 2014; Schäfer et al., 2014). In particular, the impact that led to the emplacement of the Rheasilvia basin is proposed to have occurred at the south pole with no later reorientation of the asteroid (Karimi and Dombard, 2016) directly triggering the formation of the Divalia Fossae at the equator (Bowling et al., 2014; Stickle et al., 2015). Numerical experiments show that stresses from the impact shock wave were localized in the equatorial region and caused fracturing (Bowling et al., 2014; Stickle et al., 2015). The underlying fracturing mode that is responsible for the formation of the troughs was assumed to be normal faulting (Buczkowski et al., 2012), but our recent research points to an opening-mode or mixed-mode fracture origin of the troughs (Cheng and Klimczak, 2022). The scenario described here for the formation of the Divalia Fossae by the impact that formed the Rheasilvia basin is also invoked for the Saturnalia Fossa and Veneneia impact.

The geographic relationship of the poles of planes through the troughs clustering near the center of the basin is the only observation that suggests the formation of the Divalia and Saturnalia Fossae were caused by the impacts that led to the emplacements of the Rheasilvia and Veneneia basins. The implication that arises from this scenario is that the troughs and basins must have formed simultaneously, specifically that the Divalia Fossae must have formed coevally with the Rheasilvia impact and the Saturnalia Fossae with the Veneneia impact. No cross-cutting relationships between the Divalia Fossae and Rheasilvia basin (and Saturnalia Fossae and Veneneia basin) that could provide relative ages have been documented, such that age relationships rely only on comparisons of crater frequencies on the two landform types (Cheng et al., 2021). Although the reported crater frequencies permit their simultaneous formation, large uncertainties allow for the Divalia Fossae to have formed well before or after the emplacement of the Rheasilvia basin (Cheng et al., 2021).

Moreover, stratigraphic relationships of the Rheasilvia basin with the geological units and structures in Vesta's northern hemisphere are mostly inferred from the assumed simultaneous basin formation with the Divalia Fossae. For example, the Divalia Fossae crosscut the Saturnalia Fossae and crattered highland units, which led to the inference that the Rheasilvia basin postdates these units in the global stratigraphy (Schäfer et al., 2014; Williams et al., 2014; Yingst et al., 2014). Any additional findings on the relative timing of troughs and basins, especially the Rheasilvia basin and Divalia Fossae will help better constrain the geologic history of Vesta.

The relationship between the Rheasilvia basin and Divalia Fossae plays an important role in determining the tectonic and, more broadly, the geological evolution of Vesta, as well as large impact structures on small bodies in general. That large impacts cause geologic activity far from the site of impact is not surprising, as antipodal focusing of seismic waves and ejecta is widely hypothesized to trigger volcanism or tectonics (e.g., Schultz and Gault, 1975; Williams and Greeley, 1994; Schultz and Crawford, 2011; Meschede et al., 2011). On Vesta, ancient cratered highlands and small-scale linear depressions are present near the north pole at the antipode of the Rheasilvia impact (Blewett et al., 2014), but large-scale troughs or other tectonic or volcanic phenomena are absent at the antipode (Bowling et al., 2013). “Hilly and lineated terrains” that are found at the antipodes of large basins on the Moon and Mercury (e.g., Schultz and Gault, 1975; Murray et al., 1974; Melosh and McKinnon, 1988) are also absent at the Rheasilvia or Veneneia antipodes.

Numerical studies reveal that troughs, grooves, or other lineaments could be formed by a large impact on small bodies (Asphaug et al., 1996; Benz and Asphaug, 1994), with observations on asteroid Ida corroborating this finding. However, grooves and lineaments on Ida occur in the antipodal region of a large impact structure. Prominent grooves not at the antipode of impact structures, such as those on Mars' moon Phobos, are unlikely to have an impact origin (Wilson and Head, 2015). That the Divalia Fossae are tied to an impact structure but are not localized at the antipodal region but instead at 90° from the impact distinguishes them from the Moon, Mercury, and other small bodies, and leaves open the question of why they are localized in the equatorial region of Vesta.

1.3. Goals of the study

Basin-bounding and intra-basin structures of the Rheasilvia basin have yet to be systematically and consistently mapped and described in detail using Dawn-derived photogeological datasets. A detailed structural map that documents the distribution of different structure types is the basis for further analyses that assess cross-cutting relationships among intra-basin structures as well as structural orientations and patterns. Cross-cutting relationships, orientations, and patterns of structures may reveal the deformation that took place during or after the basin was emplaced. Determining the structural outline of the Rheasilvia basin allows us to recalculate the basin center and reassess its location with respect to the Divalia Fossae. This work aims to (1) produce a detailed structural map of the Rheasilvia basin using consistent and rigorous mapping criteria, (2) quantify the orientations and pattern of basin structures with length-weighted rose diagrams in regional bins, (3) analyze the density of each type of structures and their relationships within the basin, (4) assess the cross-cutting relationships among the intra-crater structures and other structures, including impact craters and the Divalia Fossae, and (5) determine the geographic relationship of the Rheasilvia basin and the Divalia Fossae. These results will contribute towards understanding the post-emplacement Rheasilvia basin and global tectonics on Vesta.

2. Methodology

2.1. Structural mapping and quantitative analyses

We conducted structural mapping on the HAMO-based Dawn FC clear filter image mosaic that has an average resolution of 60 m/pixel (Roatsch et al., 2015). We complemented the image mosaic by calculating several hillshade maps with the shade function in the open-access USGS software ISIS3 from the ~70 m/pixel DTM (Fig. 1; Preusker et al., 2016). Our mapping was further assisted with topographic profiles in ESRI's ArcGIS software. The topographic expression of a structure is distinctly shown when the structure is perpendicular to the source of illumination on the hillshade. To capture all basin structures, we computed four hillshades for different solar azimuths (Fig. 2), including 56°E, 146°E, 124°W, and 34°W, with a fixed zenith of 45° for all hillshades.

These datasets were projected to a south-pole stereographic projection using a 255-km-diameter sphere model. We used the Claudia Double-Prime system (Li and Mafi, 2012; WGCRE, 2014), a coordinate system for Vesta adopted by the International Astronomical Union (IAU) Working Group on Cartographic Coordinates and Rotational Elements (WGCRE) since 2014¹, which assigns a positive longitude of 146° to the Claudia crater. Literature prior to that (e.g., Roatsch et al., 2012; Russell et al., 2012) use the “Claudia” system (the original coordinate system for Vesta), in which the longitude of Claudia crater is assigned as 0°.

Three types of basin structures were mapped based on their topographic expressions (Fig. 3), specifically *scars*, *ridges*, and *undefined lineaments*, which we define below. Basin structures were previously described as ridges, grooves, and scars (see section 1.1. of this manuscript), with grooves being defined by the depressions between two

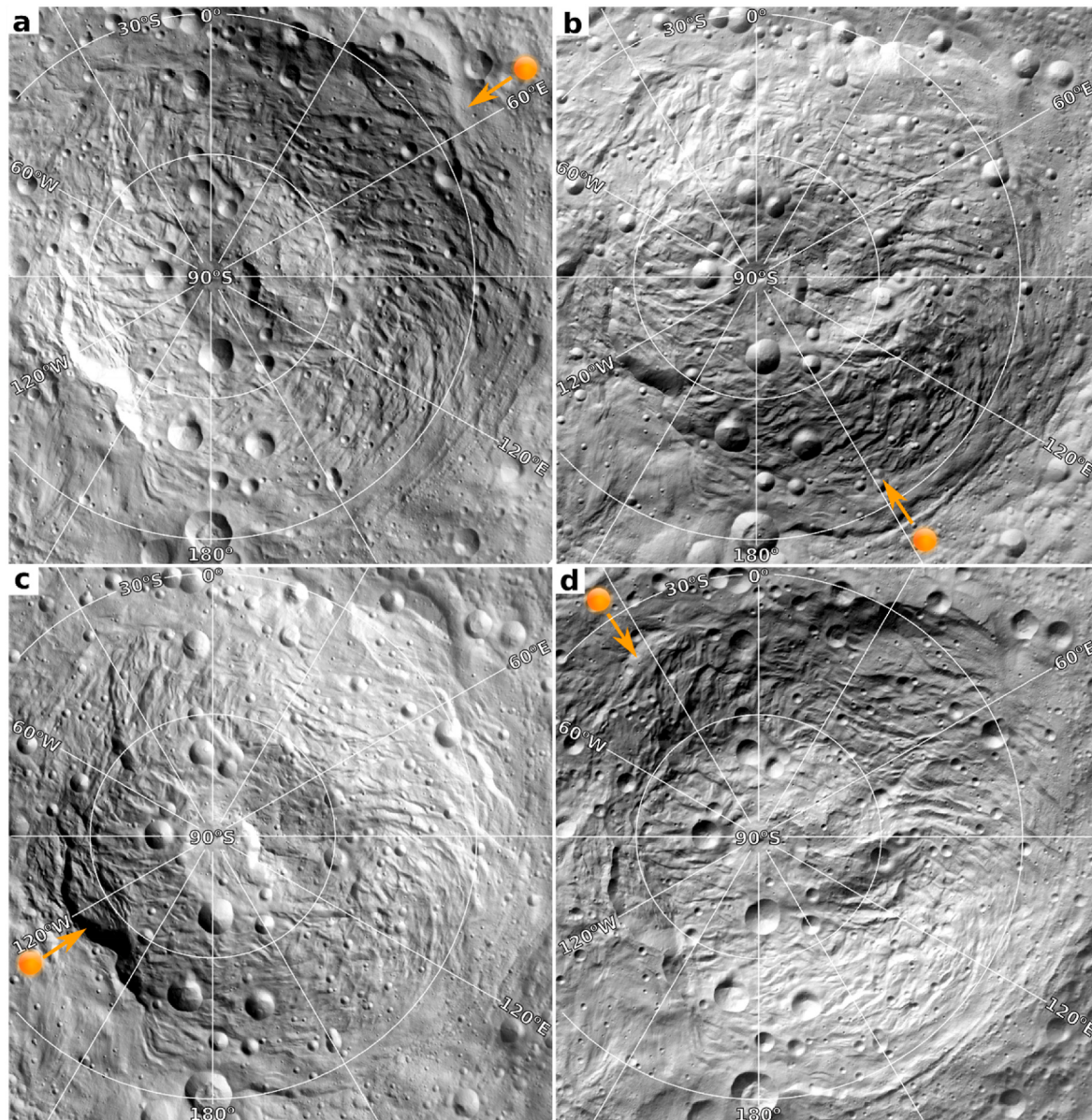


Fig. 2. Hillshade maps of Rheasilvia Basin generated from the Dawn Digital Terrain Model (DTM) with four azimuths (the angular directions of the sun) and a fixed solar incidence angle of 45°. The four azimuths we used include (a) 56°E, (b) 146°E, (c) 124°W, and (d) 34°W, which correspond to 0°, 90°E, 180°, and 90°W, respectively, in the original Claudia coordinate system for Vesta. The illumination direction is shown with an orange circle on each of the hillshades. The hillshades are in south polar stereographic projection. (For interpretation of the references to color in this figure legend, the reader is referred to the Web version of this article.)

ridges or two oppositely down-dipping scarps; thus, they are not included as a separate type of structure in this study. Apart from ridges and scarps, the surface texture of the basin is also defined by densely intersecting lineaments visible on the FC imagery, which have not been mapped before and are therefore included in our mapping.

Scarps are here defined as long and narrow linear structures that display a sharp topographic break. The scarp surface appears to be distinctively bright when facing the sun and is in the shade when facing away from the sun (Fig. 3a and b). All scarps were mapped by placing a polyline along the top of the continuous sharp topographic break as shown in the topographic profile (Fig. 3c) and presented using map symbols with the tick marks indicating the downslope direction (Fig. 3d). We further designated the most prominent scarps that define the edge of the Rheasilvia basin as *basin-bounding scarps*. These scarps are meaningful for outlining the basin perimeter, and they help define the basin center.

Ridges are defined as long, narrow, positive-relief structures. The

slope facing the illumination appears as a bright surface that gradually darkens as the slope becomes less steep near the crest with the opposite slope being in the shade or less illuminated (Fig. 3e and f). Continuous ridge crests are identified (Fig. 3g) and traced in the mapping (Fig. 3h) using map symbols with a pair of arrows pointing away from one another indicating the downslope of the two sides of the ridge. *Undefined lineaments* are linear structures that are seen on the FC images (Fig. 3i), but they are too fine to display any characteristic topographic properties in the hillshades or topographic profiles (Fig. 3j and k). These structures were mapped entirely based on the FC imagery (Fig. 3l).

All structures are mapped at a fixed map scale of 1:200,000 as polylines with regularly spaced vertices set to 1 km by using the streaming function of the ArcMap Editor to ensure equal and consistent sampling for further orientation and spatial density analyses in this work. The structural map is provided as supplementary shapefiles that can be viewed and edited in an ArcGIS environment. We analyzed the orientations and densities of each type of structure within the basin. The

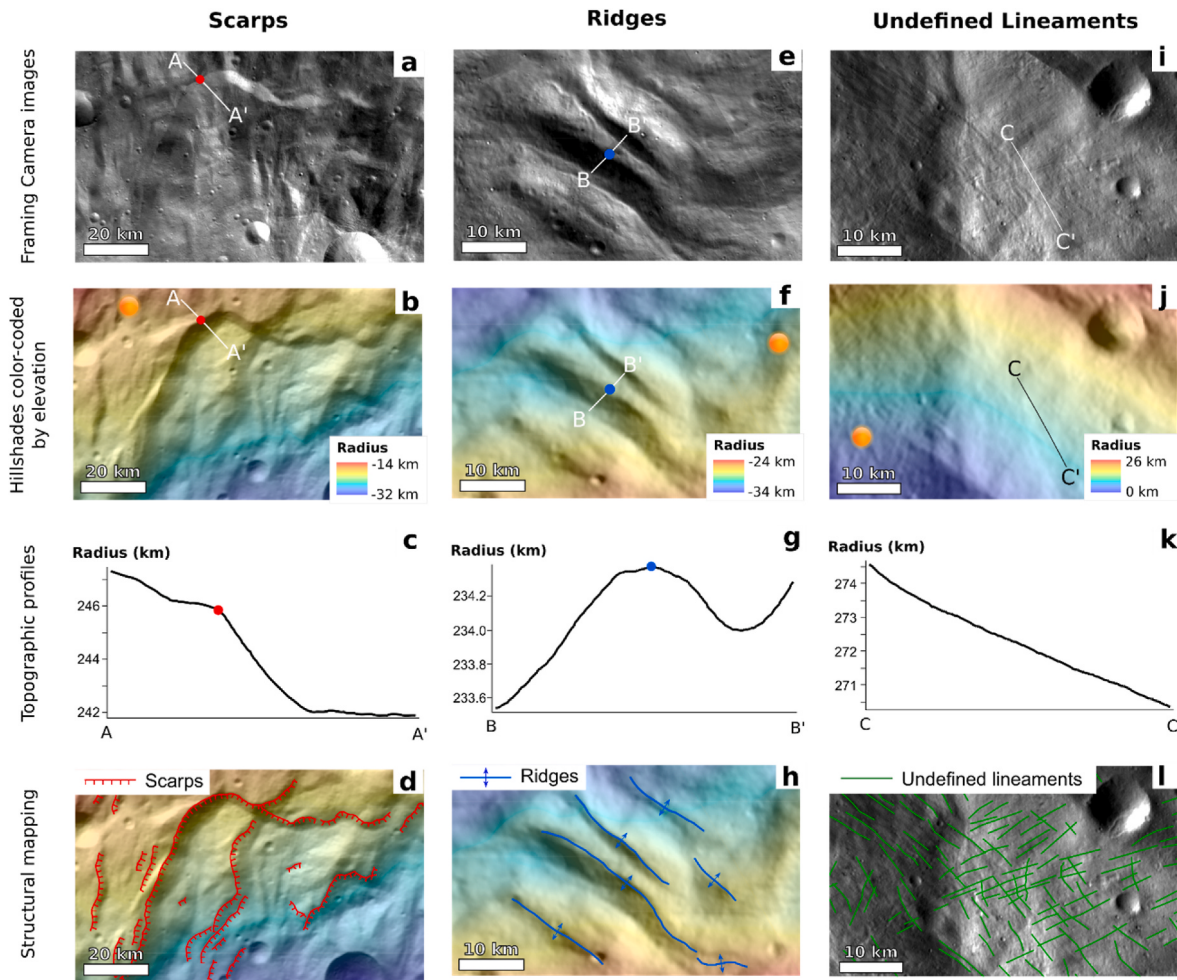


Fig. 3. Identification and classification of basin structures based on FC image, hillshades, and topographic profiles with examples of mapping. An example of scarps as seen in (a) FC images and (b) hillshades (with the azimuth of 34°W from Fig. 2d) color-coded by elevation. (c) Topographic profile A-A' across a scarp displays a sharp topographic break, marked by a red dot. The location of the profile is labeled in (a) and (b) and the point of the topographic break is also indicated as red dot in the profile. (d) Map of scarps. An example of ridges in (e) FC images and (f) hillshades (with the azimuth of 56°E from Fig. 2a) color-coded by elevation. (g) Topographic profile B-B' across a ridge displays positive relief with its crest marked by a blue dot. The location of the profile is labeled in (e) and (f) with the ridge crest also marked with blue dots. (h) Ridges are mapped on the hillshade by tracing their crests. Examples of undefined lineaments in (i) FC images and (j) hillshades (with the azimuth of 124°W from Fig. 2c) color-coded by elevation. These lineaments are visible on the FC image in (i) but are barely recognizable or invisible on the hillshade in (j). (k) Topographic profile C-C' displays no distinctive topographic properties of these lineaments. The location of the profile is labeled in (i) and (j). (l) Undefined lineaments are mapped on the FC image. All images are in south pole stereographic projection. The reference elevation is defined to be the mean planetary radius of 262 km. Refer to Fig. 1 for the locations of the examples. (For interpretation of the references to color in this figure legend, the reader is referred to the Web version of this article.)

detailed methods of these analyses will be further elaborated on in the respective sections of this paper (see sections 3.2 and 3.3).

2.2. Determination of the basin and troughs configurations

To determine the geographic relationship of the Divalia Fossae and the Rheasilvia basin, we need to determine the planes defined by the troughs and compare their poles with the previously calculated basin center. We used the dataset from Cheng and Klimczak (2022), which includes maps of all 19 trough segments of Divalia Fossae. The planes of these troughs and their poles were calculated using *Stereonet 11* (Allmendinger et al., 2013; Cardozo and Allmendinger, 2013). We subsequently computed the ellipses of two standard deviations (2σ) and three standard deviations (3σ) of the location of the poles, which are corresponding to 95% and 99.7% confidence intervals (CIs), respectively, using the built-in Kamb contouring function in *Stereonet 11*. These ellipses were then compared with the location of the central mound and two center points for the Rheasilvia basin, including our calculated

center and the original one defined by Jaumann et al. (2012), who determined the center of the basin by fitting a perfect circle to the basin. An in-depth explanation of these methods is provided in section 4 of this paper.

3. Rheasilvia basin structures

3.1. Structural map

We mapped 30 prominent basin-bounding scarps equaling a total length of 1311 km, 563 scarps within the basin with a total length of 8586 km, 494 ridges with a total length of 5814 km, and 4393 undefined lineaments with a total length of 29340 km (Fig. 4). We have also outlined the location of the central mound of the basin following outward-facing scarps that bound the local topographic high. In our mapping, we included the floors and rims of those impact craters with diameters greater than 20 km that were listed in the crater catalogue in Liu et al. (2018) to provide a full picture of the structures of the basin floor and to

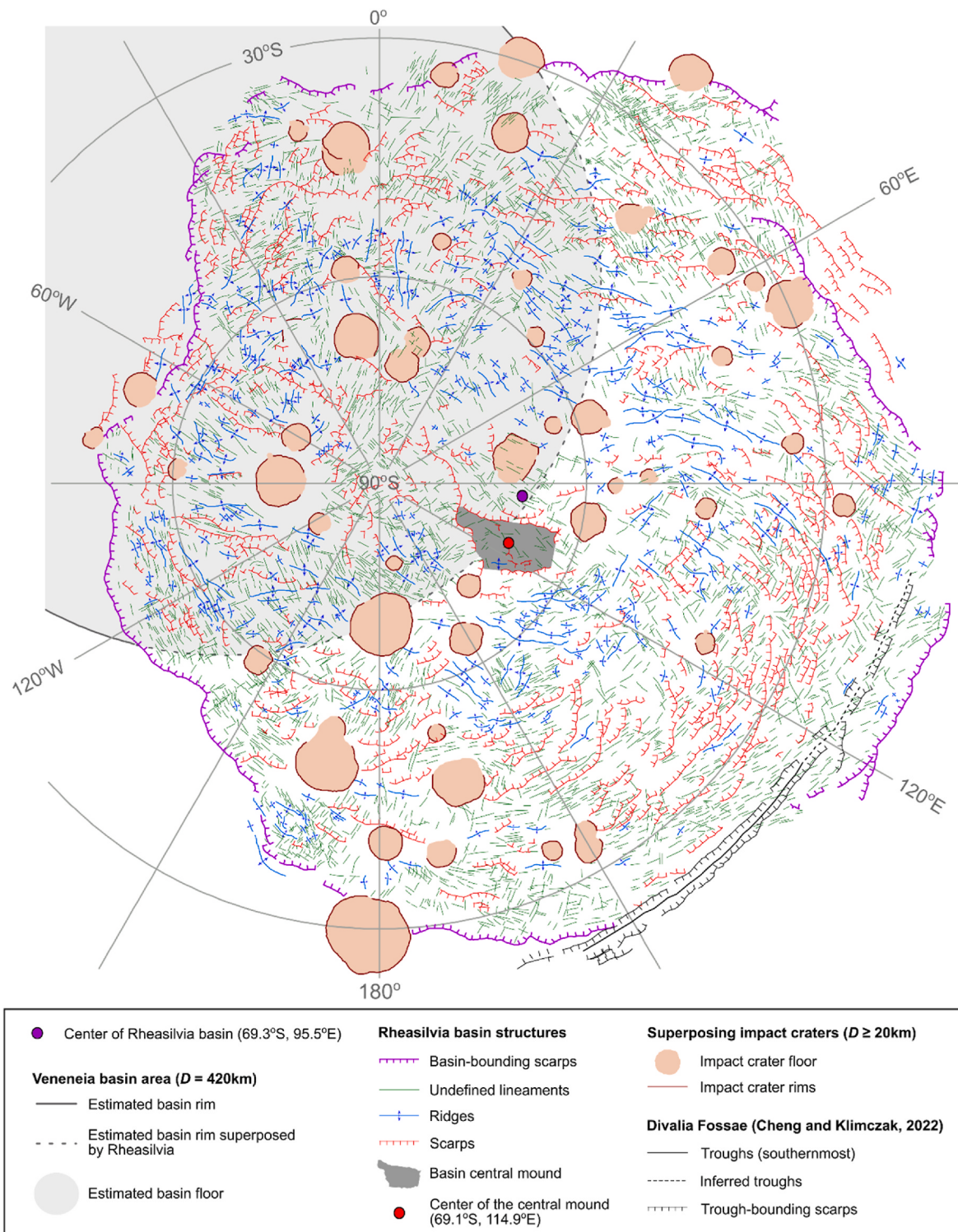


Fig. 4. Structural map of the Rheasilvia basin. The geometric mean center of the basin is calculated from the basin-bounding scarps and plotted as a purple dot. The geometric mean center of the central mound is calculated from the area outlined by scarps bordering the local topographic high in the basin center, it is displayed with a red dot. Refer to the text for the definition of structural map units. The map is in south polar stereographic projection. (For interpretation of the references to color in this figure legend, the reader is referred to the Web version of this article.)

investigate cross-cutting relationships between the craters and structures. We also included the troughs and their bounding scarps of the Divalia Fossae from Cheng and Klimczak (2022) in the structural map of this research to explore their potential cross-cutting relationships with basin.

The basin is asymmetrically hexagonal and outlined by basin

bounding-scarsps, consistent with previous study (Schenk et al., 2012). We calculated the geometric mean center of the basin based on the basin-bounding scarps and estimate it at 69.3°S and 95.5°E (Fig. 4). Our calculated center somewhat differs from the basin center of 75°S and 87°E of Jaumann et al. (2012), who defined the center by fitting a perfect circle to the basin structure and did not account for the true basin

shape. Both centers are located near the central mound of the Rheasilvia basin. From the mapped outline of the central mound, we also calculated its geometric mean center to be located at 69.1°S and 114.9°E (Fig. 4), which is very close but not coincident with the basin centers. We estimated the extent of the Veneneia basin that is superposed by the

Rheasilvia basin as a circle using the three-point method in the *CraterTools* plug-in (Kneissl et al., 2011) by identifying three points along the preserved basin scarps. The resulting circular area has a ~420 km-diameter (Figs. 1 and 4), consistent with the widely accepted estimated size of Veneneia basin (e.g., Jaumann et al., 2012; Marchi et al., 2012;

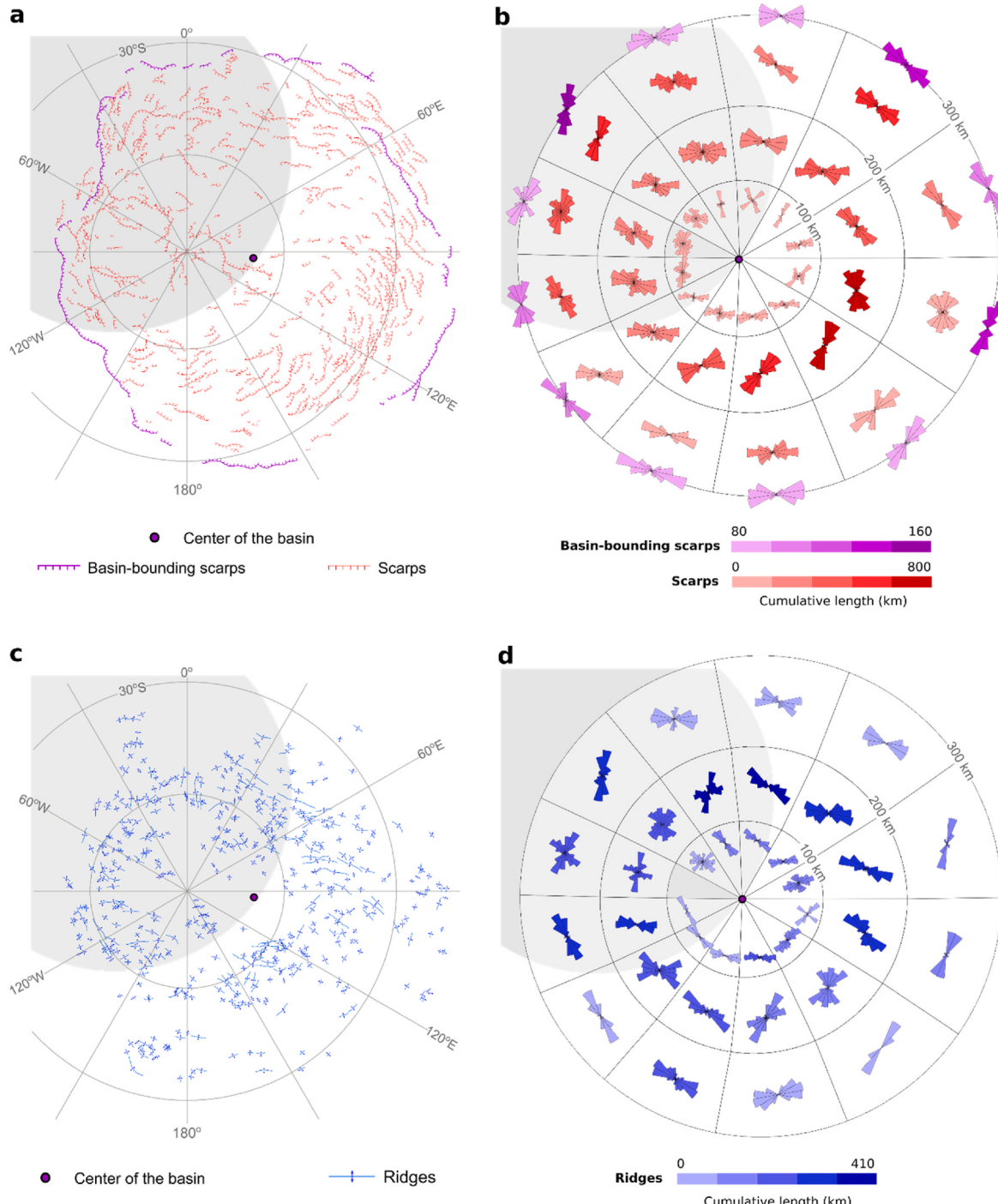


Fig. 5. Structural units shown on separate maps on the left with their orientations presented as rose diagrams on the right. The basin was binned by three concentric circles with radii of 100 km, 200 km, and 300 km from the geometric mean center of the basin (purple dot) and further divided by 12 lines radiating from the center with an equal angle of 30°, resulting in 36 bins (outlined in black). As with previous maps (Figs. 1 and 6), the estimated Veneneia basin floor is shaded in grey. (a) Basin-bounding scarps (purple) and scarps as they occur in the basin (red). (b) Length-weighted rose diagrams are plotted for each bin, with color variation showing their cumulative lengths for the basin-bounding scarps in purple and scarps within the basins in red. (c) Ridges (blue) as they occur on the map. (d) Length-weighted rose diagrams of ridges are plotted for each bin, with variations of intensity of the blue indicating their cumulative lengths. (e) Undefined lineaments (green) as they occur on the map. (f) Length-weighted rose diagrams of the undefined lineaments are plotted for each bin, with the intensity of the green color indicating the cumulative lengths. All maps are in south polar stereographic projection. (For interpretation of the references to color in this figure legend, the reader is referred to the Web version of this article.)

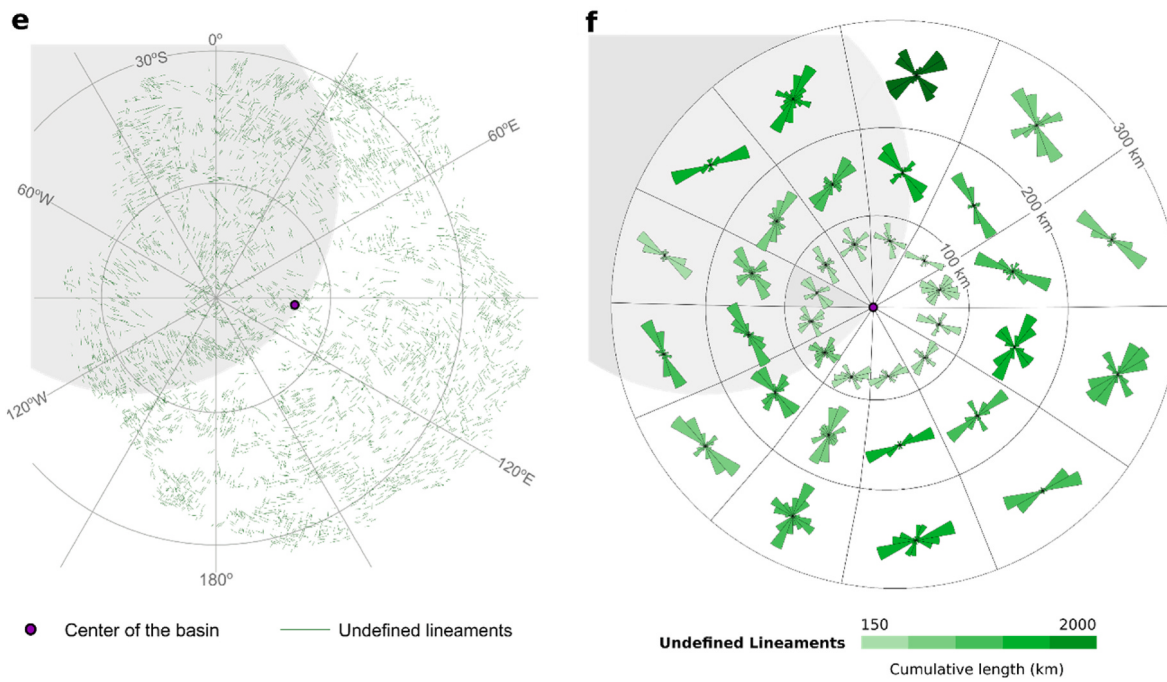


Fig. 5. (continued).

Schenk et al., 2012).

Visual inspection of our mapped structures reveals a partly preserved clockwise spiral pattern of basin structures extending from the central mound to the rim (Fig. 4). The pattern is most distinctly expressed by scarps and ridges, but some lineaments also follow the same structural trend on the Rheasilvia basin floor outside of the estimated area of the Veneneia basin floor. Scarps mostly face the basin center along and near the basin-bounding scarps. There, they show a pattern concentric to the basin center, but they systematically deviate from this concentric pattern closer to the center of the basin. This pattern is the most distinct and systematic in the eastern part of the basin between 60°E to 150°E. The occurrence of ridges is sparse near the basin-bounding scarps at 0° to 60°E and 120°E to 180°, but they are densely distributed at the low-lying basin floor between the central mound and basin slope. Some ridges follow the spiral pattern of the scarps, such as the curved ridges observed at 60°E to 120°E. The pattern of scarps and ridges is less systematic at the western part of the basin at 30°W to 120°W, which we attribute to pre-existing structure in the Veneneia basin (Fig. 4). Although some undefined lineaments follow the orientations of scarps and ridges locally, they generally do not follow the spiral pattern.

3.2. Orientation of each type of structure

To assess the orientation of each type of structure, the basin was subdivided into bins using three concentric circles with radii of 100 km, 200 km, and 300 km from the calculated basin center. Those concentric bins were subdivided into 12 radial bins, resulting in 36 regional bins around the basin center. Length-weighted rose diagrams were plotted for the three types of structures in each bin to visualize their orientations across the basin to aid our assessment of the structural patterns (Fig. 5).

The basin-bounding scarps are large concentric structures around the basin center as seen on both the structural map and rose diagrams (Fig. 5a and b). Deviations from the concentric pattern are most pronounced in those parts of the Rheasilvia basin that superpose the Veneneia basin. The intra-basin scarps form a pervasive spiral pattern within the basin, especially near the basin-bounding scarps (Fig. 5a). The rose diagrams quantitatively capture the spiral pattern with the scarps furthest from the basin center showing distinctively concentric

orientations, but their orientation increasingly and systematically deviates from this concentric orientation closer to the basin center (Fig. 5b).

Ridges are less prominent than scarps, as they have shorter individual lengths and their pattern relative to the basin center is not as well defined as the scarps (Fig. 5c). Overall, the ridges show concentric and, in a few places, radial orientations to the basin center with concentric orientations mostly near the basin-bounding scarps (Fig. 5d). There are regional bins that show ridge orientations like those of the scarps (Fig. 5b), but they do not form an obvious spiral pattern throughout the basin. The ridges between latitudes of 30°S to 60°S and longitudes of 0° to 90°E show a regional fabric trending roughly from east and west (Fig. 5c). This pattern is also captured by the rose diagrams with a high density of ridge segments (Fig. 5d).

Undefined lineaments are widely and densely distributed across the basin floor (Fig. 5e). Most are relatively short compared to ridges and scarps, and they form no distinctive map patterns. Rose diagrams show that the undefined lineaments display preferred orientations in all regional bins (Fig. 5f). There are regional bins that show radial and concentric patterns with respect to the basin center, but they do not form a consistent pattern across all bins, such that no systematic pattern is present throughout the basin. Some undefined lineaments between the latitudes of 30°S to 60°S and longitudes of 0° to 90°E mimic the regional fabric of ridges (Fig. 5c) trending roughly from east and west (Fig. 5e).

Lighting may potentially impose a bias on the detectability of structures. Where solar illumination is parallel to the structure, the contrast in illumination of the structure is so low as to render the structure nearly invisible, whereas a structure approximately perpendicular to this direction is prominently visible on the FC images. The mapping of scarps and ridges was verified with hillshades created from multiple azimuths (Figs. 2 and 3a-h), but the undefined lineaments could not be verified (Fig. 3i-l). Thus, the preferred orientations of ridges and scarps have no or minimal lighting bias and can be accounted for by the tectonics of the basin. However, preferred orientations of undefined lineaments may be biased by the lighting of FC images, and they may not fully characterize the tectonics of the basin.

3.3. Density of structures

We analyzed the density of each type of structure within the Rheasilvia basin. Each structure was split at its vertices into ~1 km long segments. The splitting ensures that longer structures are more prominently represented in our density calculation because longer structures will return more segments. The coordinate of the centroid of each segment was calculated, and the number of centroids per square kilometer was computed for each type of structure using the *Kernel Density Calculates function* in ArcMap, which calculates the density of point features around each output raster cell in an equal area stereographic projection. Basin-bounding scarps were not considered for this calculation, as they would weigh scarps more heavily along the basin boundary.

Basin structures are densely distributed across almost the entire basin floor. Some areas near post-Rheasilvia impact craters or at the downslope of scarps (e.g., Matronalia Rupes and the central mound-bounding scarps) show only undefined lineaments or no structures (Figs. 4 and 6). These smoother areas are possibly covered with resurfaced materials produced by impacts or by landslides. The density of the scarps is highest between 80°E to 150°E along the latitude of 30°S. The scarps have a high density (dark red in Fig. 6a) on the basin floor that slopes toward the basin center, where they are associated with the basin-bounding scarps, and they show a low density on the flat basin floor near the central mound (light red in Fig. 6a).

Ridges show a low density near the central mound and near the basin-bounding scarps (light blue in Fig. 6b) but they cluster between these two regions on the flat basin floor (dark blue in Fig. 6b), encircling the central mound. Hence, scarps and ridges show an opposite spatial distribution, with scarps densely located near the basin perimeter surrounding a group of ridges at the basin floor around the central mound (Fig. 6a and b). Undefined lineaments show a less distinct pattern in their spatial density with some of them densely located near the basin-bounding scarps (Fig. 6c). Regions of low structural density occur where superposed impact craters are recorded, and thus resurfacing has occurred and erased the expressions of this structure type.

3.4. Cross-cutting relationships

The three types of structures in the Rheasilvia basin lack a systematic pattern of cross-cutting relationships. An example of an area displaying wide variation in cross-cutting relationships is shown in Fig. 7. These relationships (all labeled in Fig. 7c) include one basin-bounding scarp truncating a large scarp within the basin (1), that large scarp cutting smaller scarps (2) and ridges (3), and a ridge abutting that large scarp (4). Such mutually cross-cutting relationships are present across the entire basin floor (Fig. 6), indicating that all these structure types formed simultaneously and not sequentially.

Scarps and ridges are in all cases superposed by impact craters (Fig. 4), indicating that the structures were formed before any of the craters were emplaced. Most undefined lineaments are also superposed by impact craters, and only 34 out of 4393 of the lineaments (0.77%) cross-cut crater floors (Fig. 4). This shows that most lineaments were formed before the emplacement of the craters, but also that their formation continued locally for some time.

The southernmost trough belonging to the Divalia Fossae cuts the Rheasilvia basin-bounding scarps and lies partly within the basin. The relationship is most obvious in the hillshade images (Fig. 2b,d) that differ the most in illumination conditions as compared to the natural lighting in the FC images. The trough is not cut by any of the scarps and ridges, but it is cut by undefined lineaments (Fig. 4). That the trough cuts the basin-bounding scarp and basin floor but is not cut itself by scarps and ridges indicates that the trough formed after the emplacement of the Rheasilvia basin and after the formation of all major basin interior structures. This heretofore unrecognized cross-cutting relationship adds crucial information to the interpretation of the origin of the troughs. We will explore the basin and trough relationship further in the next section.

4. Spatial relationship of Rheasilvia basin and Divalia Fossae

With no cross-cutting relationships previously described, the Rheasilvia basin and Divalia Fossae were widely considered to be genetically linked because of the spatial correlation of the basin center with the poles to vertical planes projected through the troughs. We have plotted the Divalia Fossae and their associated pit-crater chains from Cheng and Klimczak (2022) with the Rheasilvia basin-bounding scarps and basin center of this study (Fig. 4). This map highlights the spatial relationship of the basin and troughs that include the southernmost trough of the Divalia Fossae cutting into the Rheasilvia basin. This newly recognized cross-cutting relationship suggests that this trough was formed after the emplacement and modification of the Rheasilvia basin.

The series of parallel troughs of the Divalia Fossae were recognized as parts of a single structure with a common origin (e.g., Buczkowski et al., 2012; Jaumann et al., 2012; Scully et al., 2014; Schäfer et al., 2014). Furthermore, all of the major troughs are consistent with one another with regards to their map patterns and degradation (Cheng and Klimczak, 2022). They are all superposed by impact craters with no pre-existing craters found within the troughs (Cheng et al., 2021). These observations further suggest that the series of troughs were formed at the same time. Taking together this timing relationship and the cross-cutting relationship between the Divalia Fossae and Rheasilvia basin, the entire Divalia Fossae structure has to be formed after the emplacement and modification of the Rheasilvia basin.

The Divalia Fossae do not show an obvious concentric arrangement around the Rheasilvia basin center nor the central mound when viewed in stereographic projection centered on the south pole (Fig. 8). To better evaluate their arrangement, we determined the planes defined by the Divalia Fossae using two methods and plotted their poles with respect to the basin centers on an equal-area stereonet (Fig. 9). *Method 1* follows the procedure described in Jaumann et al. (2012), in which the planes defined by the troughs are assumed to be vertical, cutting through the center of the asteroid. The orientations of the planes located at the center positions of each of the trough segments are shown as great circles in an equal area stereonet (Fig. 9a). The poles of the trough-defined planes are clustered around the center of the stereonet, consistent with the result from Jaumann et al. (2012).

We plot the confidence interval ellipses of the poles of the troughs in shades of grey. The confidence interval ellipse describes the uncertainty inherent in the estimate of the pole position, and it represents the set of acceptable hypotheses. For example, if a basin center lies outside of a 95% confidence interval, it can be rejected (i.e., the difference is statistically significant) with 95% confidence. The two basin centers determined by Jaumann et al. (2012) and this study, as well as the center of the central mound, all lie outside of the 95% confidence interval of these poles, but the south pole of Vesta lies within it. Therefore, the south pole can be regarded as consistent with the poles to the troughs, but the basin center and center of the central mound cannot. Even for highly conservative 99.7% confidence intervals (corresponding to ± 3 standard deviations), the centers of the basin and central mound can be rejected as being consistent with the locations of the poles of the troughs.

Since the planes defined by the Divalia Fossae troughs may not cut through the center of the asteroid, we also use *Method 2*, which determines the planes defined by the troughs without the assumption that they cut through the center of the asteroid. The trough segments of Divalia Fossae belong to four main trough structures (Fig. 9; Cheng and Klimczak, 2022), and we use those four structures to redefine the planes. To determine the circular shape that best fits each structure, we used the three-point method in the *CraterTools plug-in* (Kneissl et al., 2011) that has a built-in projection correction by identifying the starting, middle, and ending points along the four structures. These circular planes are represented as small circles on an equal-area stereonet (Fig. 9b), showing that these planes do not cut through the center of the asteroid. We calculated the center locations of these circular planes to plot their

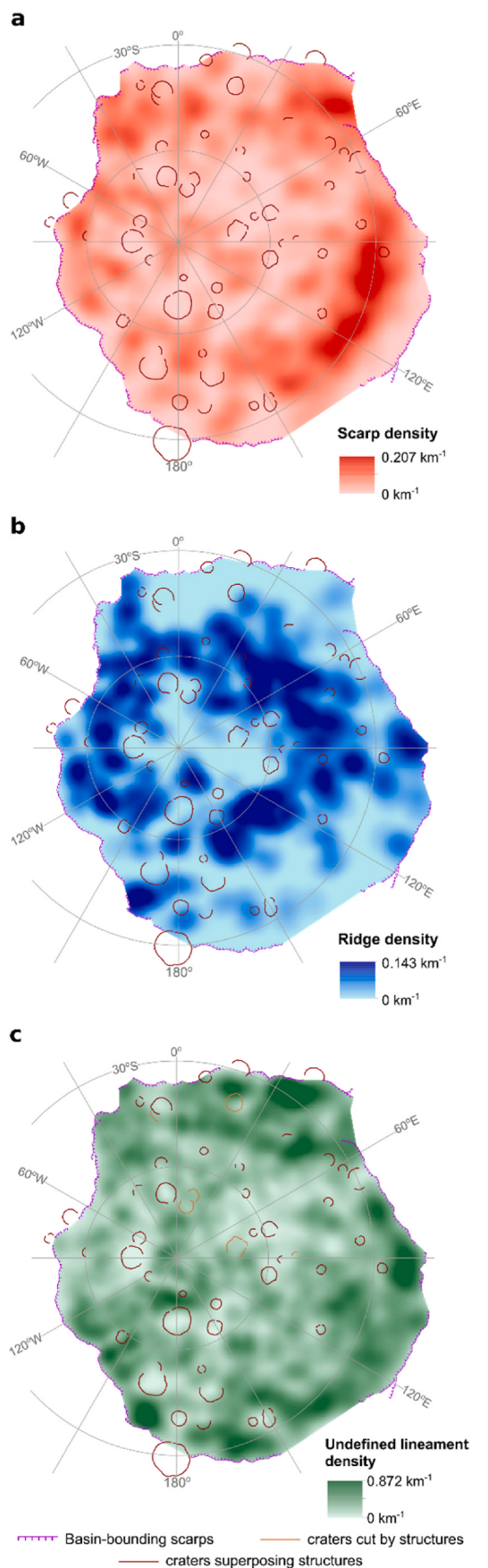


Fig. 6. Structure density maps shown for (a) scarps in red, (b) ridges in blue, and (c) undefined lineaments in green across the Rheasilvia basin outlined by the basin-bounding scarps. Structural density is expressed in kilometers of structure length per square kilometers (km^{-1}) with darker colors representing a higher density across the basin. Rheasilvia basin-bounding scarps are shown in purple. The rims of post-Rheasilvia craters that superpose the structure type are outlined in dark brown, and those that are cut by the structure type are outlined in light brown. All impact craters superpose scarps and ridge in (a) and (b). Some impact craters are cut by undefined lineaments, whereas some impact craters superpose the undefined lineaments in (c). (For interpretation of the references to color in this figure legend, the reader is referred to the Web version of this article.)

poles. The poles of the trough-defined planes cluster near the center of the stereonet, which coincides with Vesta's south pole. Like the results for *Method 1* (Fig. 9a), the two basin centers and the center of the central mound all lie outside of the 95% confidence interval of the poles, but the south pole of Vesta lies within it. Even for highly conservative 99.7% confidence intervals, the centers of the basin and central mound can be rejected as being consistent with the poles of the troughs. The basin center from Jaumann et al. (2012) lies just within the 99.7% confidence ellipse but close to the margin. As such, the observed poles to the troughs are inconsistent with the locations of the basin and central mound centers, but they are consistent with the south pole.

Troughs and basin-bounding scarps indicate that the Divalia Fossae are not concentrically arranged around the Rheasilvia basin center or around its central mound (Fig. 8). Furthermore, our structural analysis indicates that the basin center does not fall within the 95% confidence limit of the poles of the troughs, irrespective of the method used to determine the poles of the troughs and what coordinates define the basin center. As such, the locations of the poles to the troughs are inconsistent with the Rheasilvia basin center. These lines of evidence indicate that the Rheasilvia basin and the Divalia Fossae do not show a clearly defined spatial relationship with one another.

5. Discussion

5.1. Basin structures and their formation processes

The structural map of the Rheasilvia basin presented in this study (Fig. 4) allows us to conduct spatial analyses and assessments of the orientation of several types of structures found in and around this large impact structure. These results of our analyses have implications for the geologic processes that took place within the basin. Basin-bounding scarps, such as Matronalia Rupes, are interpreted as the main scarp resulting from major mass-wasting events (Otto et al., 2013). Numerous scarps within the basin represent ruptures along which slumping took place, with ridges in the front of the slump representing the toes of the slumping masses (Otto et al., 2013). This interpretation is consistent with our observation that the scarps facing the basin center are clustered near the basin-bounding scarps at the perimeter of the Rheasilvia basin (Fig. 6a), and the spatial density of ridges is higher closer toward the basin center on the basin floor around the central mound (Fig. 6b), displaying an anti-correlation in their spatial distribution. This indicates the mass movement of basin material from the basin rim towards the floor, which is likely caused by the gravitational collapse and modification during the modification stage of basin formation. This interpretation is supported by the detailed observations of the nature and orientations of mass-wasting landforms within the basin (Otto et al., 2013).

The scarps and ridges are mutually cross-cutting across the basin (Figs. 4 and 7), indicating that there were mass-wasting events across the basin without a sequence of events or specific temporal order of the mapped structure types. Since the scarps and ridges are all superposed by impact craters inside the basin (Fig. 4), they must have formed prior to the superposition of the impact craters, likely soon after the

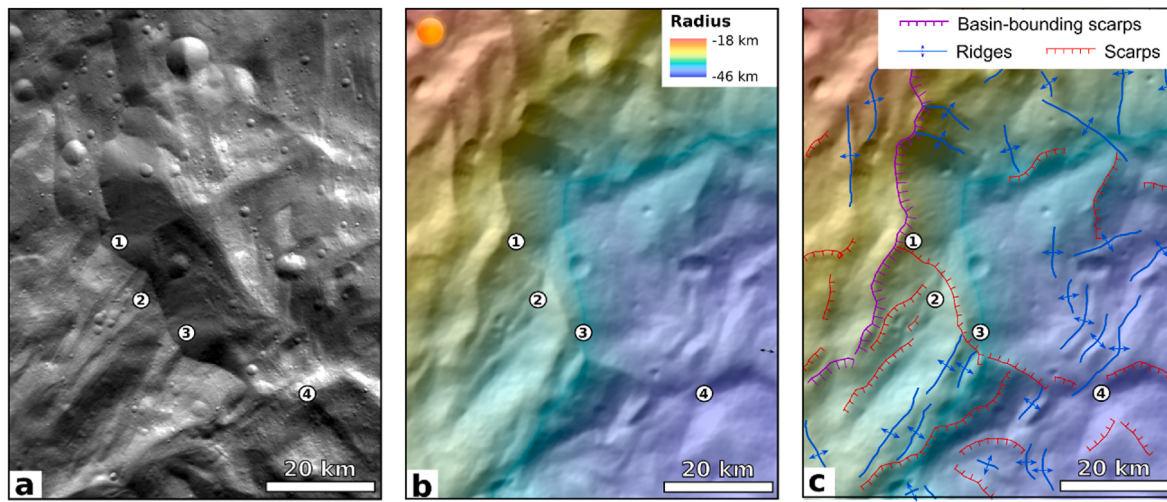


Fig. 7. A representative area showing multiple examples of cross-cutting relationships between basin-bounding scarps, scarps within the basin, and ridges labeled by numbers. (a) FC image and (b) hillshade color-coded by elevation of an area displaying complex cross-cutting relationships of structures, including (1) a basin-bounding scarp cutting scarps within the basin, a large scarp cutting (2) smaller scarps and (3) ridges, and (4) a ridge cutting a scarp. No systematic cross-cutting relationships among the different structural units are observed across the basin. The images are in south pole stereographic projection. The reference elevation is defined to be the mean planetary radius of 262 km. Refer to Fig. 1 for the image location. (For interpretation of the references to color in this figure legend, the reader is referred to the Web version of this article.)

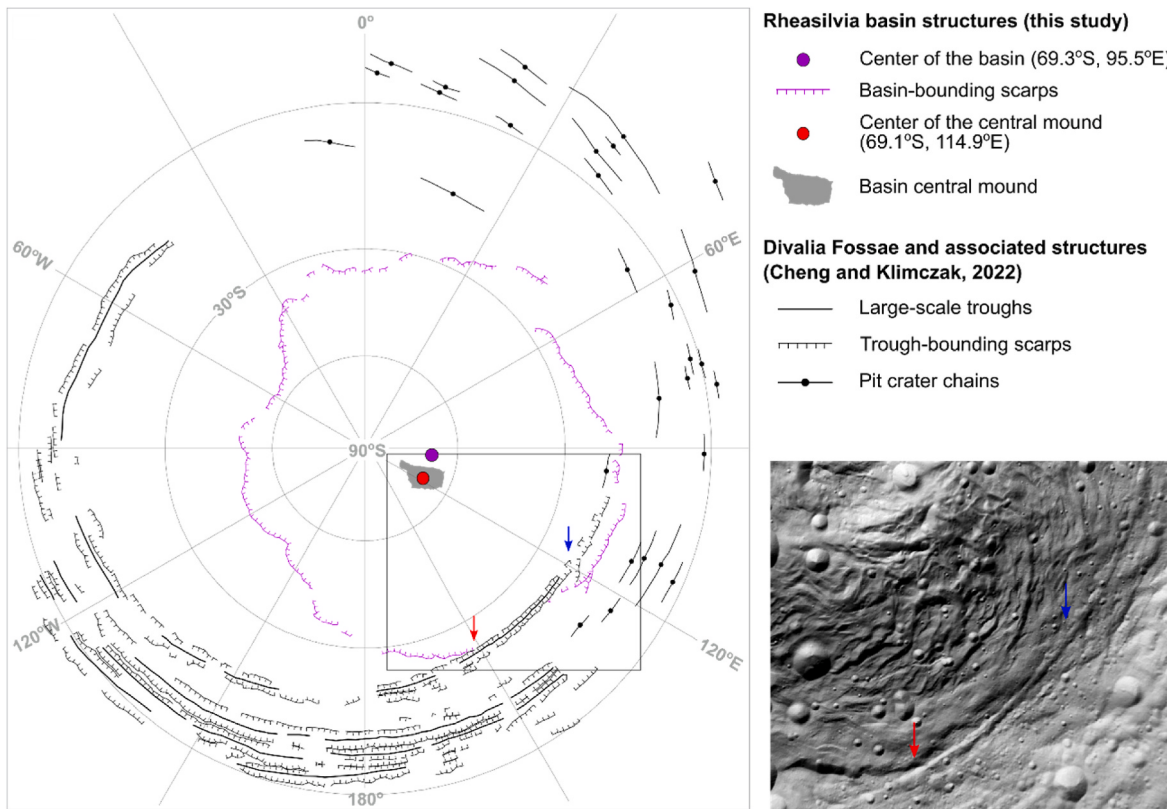


Fig. 8. Structural map (left) and hillshade (right) showing the basin-bounding scarps of the Rheasilvia basin with Divalia Fossae mapped by Cheng and Klimczak (2022). The southernmost trough is cutting the basin-bounding scarps (marked with a red arrow) and lying within the basin (marked with blue arrow). The geometric mean center of the basin is plotted on the map with a purple dot to show its configuration with Divalia Fossae. The outline of the central mound is shaded in grey with its geometric mean center plotted as a red dot. Pit-crater chains associated with the troughs on Vesta are also shown on the structural map. The hillshade image (with the azimuth of 146°E from Fig. 2b and its extent outlined in black lines on the structural map on the left) captures the cross-cutting relationship of the southernmost trough of Divalia Fossa and the Rheasilvia basin-bounding scarps with the red and blue arrows. Refer to Figs. 1 and 2 for the hillshade and elevation data. (For interpretation of the references to color in this figure legend, the reader is referred to the Web version of this article.)

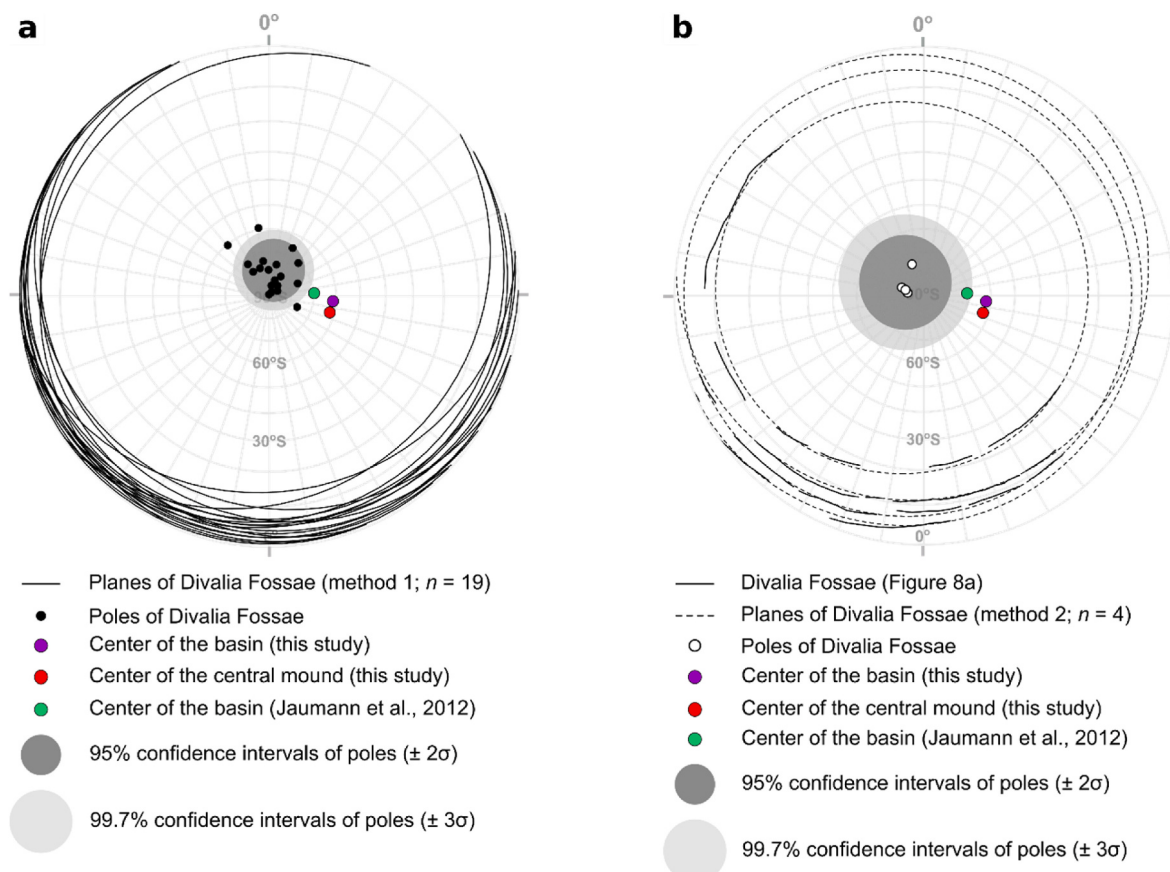


Fig. 9. Equal area south pole projection stereonet showing the configuration of the Rheasilvia basin and Divalia Fossae. (a) The configuration of the Rheasilvia basin and Divalia Fossae is investigated using method 1 by Jaumann et al. (2012). Planes are defined by the center positions of the trough segments mapped by Cheng and Klimczak (2022), represented by great circles shown in black. The center of the Rheasilvia basin calculated in this study and from Jaumann et al. (2012) are plotted as purple and green dots, respectively. The center of the central mound calculated in this study is plotted as a red dot. The poles of the trough-defined planes are plotted in black. Confidence ellipses corresponding two standard deviations (95% confidence interval (CI)) and a very conservative three standard deviations (99.7% CI) of these poles are calculated and highlighted in dark grey and light grey, respectively. (b) The configuration of the Rheasilvia basin and Divalia Fossae is investigated by defining small circles of the main trough structures (method 2). The 19 trough segments of Divalia Fossae (black lines) belong to four main structures (Cheng and Klimczak, 2022). The planes that best fit each of the four structures are presented as small circles in dashed lines with their poles shown as white dots. The two standard deviations (2σ ; 95% CI) ellipse and three standard deviations (3σ ; 99.7% CI) ellipse of these poles are calculated and highlighted in dark grey and light grey, respectively. The reader is advised that we applied the new coordinate system used for Vesta updated in 2014¹¹, which is different from the one used by Jaumann et al. (2012).

(For interpretation of the references to color in this figure legend, the reader is referred to the Web version of this article.)

emplacement of the Rheasilvia basin, with most mass wasting being complete shortly after basin formation. Otto et al. (2013) reported young slides and slumps at the Matronalia Rupes scarp and suggested they demonstrate the ongoing collapse of the basin. However, we find that this interpretation is not representative of the majority of mass-wasting that occurred in the basin.

Scars display a well-preserved spiral pattern between 60°E and 150°E , coinciding with the area that does not superpose the Veneneia basin floor (Fig. 5a and b). The spiral pattern is consistent with previous works in as far as it is clockwise extending from the central mound to basin rim. One possible explanation for this structural pattern is that the curved structures are remnants of the basin-collapse process when materials moving from the rim to the floor radially were deflected by the Coriolis effect (Jutzi et al., 2013; Otto et al., 2013, 2016). Otto et al. (2016) interpreted the spiral patterns as ‘curved ridges’ of materials deposited along the predominant slope from the basin rim to the floor during the basin modification stage. The velocities of mass movement derived along these ‘curved ridges’ were calculated by assuming they were caused by the Coriolis effect (Otto et al., 2016), which generally agrees with the predicted mass motion velocity from numerical simulations (Jutzi et al., 2013). These ‘curved ridges’ on a large-scale map

consist of scarps and ridges based on our structural map (Fig. 4). If the scarps represent rupture during slumping and the Coriolis effect is responsible for the spiral pattern, the Coriolis force may not just deflect the movement of slumping materials but also influence the preceding rupture during basin collapse.

However, the spiral pattern of the Rheasilvia basin should be expected to extend from the south pole of Vesta under the Coriolis effect, instead of the center of the impact basin. From the preserved structures we mapped, it is impossible to distinguish if the spiral pattern is centered around the south pole or the Rheasilvia basin (Fig. 4). Schenk et al. (2022) reported that spiral patterns are common to complex craters on Moon, Mars, Mercury, Ceres, and other icy bodies, which are not located near the poles. As such, the Coriolis effect does not need to be invoked to form the spiral pattern on the Rheasilvia basin. The crater examples given by Schenk et al. (2022) range in diameter from 9 to 66 km, which are much smaller than the 450-km-diameter Rheasilvia basin, and they thus have much lower size ratios relative to their parent bodies. Furthermore, the reported spiral patterns in these smaller craters were selected from visual inspection without structural analysis and they are mostly partially preserved, as the crater floors are buried by impact melt and debris. Therefore, these craters are likely not analogous to the

Rheasilvia basin and its pervasive spiral deformation pattern, leaving the Rheasilvia spiral pattern as uncommon among large impact structures in the solar system.

The spiral pattern is not present at the western extent of the Rheasilvia basin, where it is estimated to superpose the Veneneia basin (Fig. 4). Any pre-existing Veneneia basin structures likely substantially influenced the orientations of structures in the Rheasilvia basin. In this case, the Veneneia basin floor and its structures would have been planes of weakness during the Rheasilvia impact. Thus, Vesta's lithosphere must have been highly fractured by the Veneneia impact, and it remained highly fractured until the Rheasilvia basin was emplaced. Any fracture healing and fracture annealing caused by shock residual or interior heat is therefore unlikely to have occurred on the Veneneia basin floor. This absence is possible if the Veneneia basin formed from a low-velocity impactor, similar to that proposed for the Rheasilvia impact (O'Brien and Sykes, 2011). This scenario is consistent with the lack of a melt sheet associated with the Veneneia impact on the preserved part of the basin.

5.2. Origin of the Divalia Fossae

The Divalia Fossae are widely accepted to have formed directly by the impact that formed the Rheasilvia basin (e.g., Buczkowski et al., 2012; Jaumann et al., 2012; Scully et al., 2014; Schäfer et al., 2014; Williams et al., 2014; Yingst et al., 2014). This scenario solely relied on the geographic relationship that the Divalia Fossae showed with respect to the center of the Rheasilvia basin (Jaumann et al., 2012; Scully et al., 2014; Schäfer et al., 2014). And although numerical modeling of the Rheasilvia impact suggests that extension is expected at the equatorial region when invoking the presence of a ductile core and other specific interior characteristics (Bowling et al., 2013), it is unknown if Vesta's interior properties are consistent with the modeling parameters and/or if the predicted extension is consistent with the magnitude of strain and orientation of the observed troughs. Thus, the collocation of the troughs and basin center remains the only direct geological support of the hypothesis.

Our reassessment of this geographic relationship indicates with upward of 95% confidence that the geometric mean centers of the basin and central mound both are not co-located with the poles of the Divalia Fossae (Fig. 9) and that a collocation with the south pole is more probable. This result establishes that the Divalia Fossae do not display a clearly defined geographic relationship with the Rheasilvia basin. Due to the interior heterogeneities, geometry of the impact, and/or deformation mechanics, the Rheasilvia basin center would not necessarily have to coincide with the poles of troughs for them to be genetically linked. But the lack of a clear collocation of the basin center and troughs weakens the sole argument on which the hypothesis, by which the basin-forming impact triggered the formation of the troughs of Divalia Fossae, is based on.

The previously proposed origin of the troughs is further challenged by the newly identified cross-cutting relationship that the Divalia Fossae and Rheasilvia basin-bounding scarps display. The southernmost trough of the Divalia Fossae cuts the basin-bounding scarp and lies partly within the basin without being crosscut by the scarps and ridges in the basin interior (Figs. 4 and 8), indicating that the troughs must be formed after the emplacement and modification of Rheasilvia. The emplacement and immediate modification of the Rheasilvia basin were estimated to take place over approximately 2–3 h (Jutzi et al., 2013; Ivanov and Melosh, 2013; Otto et al., 2016), which is when near-surface downhill mass motion of highly shocked and fractured material occurred radially from the crater walls toward the basin floor (Schenk et al., 2012; Otto et al., 2013; Jutzi et al., 2013), also marking by the formation of the basin-bounding scarps. In contrast, typical earthquake rupture

propagation rates of approximately 3 km/s (Stein and Wysession, 2009) imply that fractures that formed deep within Vesta from the Rheasilvia impact propagated to the surface after ~100–150 s (Stickle et al., 2015), but with seismic shaking affecting the surface possibly for hours. Following the results of these studies, the formation of Divalia Fossae, if indeed caused by the Rheasilvia impact, would have to take place before or within the same timeframe of the modification stage of the Rheasilvia basin, which contradicts the observed cross-cutting relationship. As no impact crater, other than the Rheasilvia basin, are observed to be cut by the Divalia Fossae (Cheng et al., 2021), the structures are also unlikely to have first formed with the basin but experienced a later joint or fault reactivation to cause the present cross-cutting relationship with Rheasilvia. Hence, our geologic observations suggest that it is likely for the Divalia Fossae to be formed after the basin modification stage, questioning the previously proposed impact-induced origin of the Divalia Fossae.

It is widely accepted that large impacts can form major structures at the antipodes (e.g., Schultz and Gault, 1975; Murray et al., 1974; Melosh and McKinnon, 1988); however, no such structures on Vesta and Divalia Fossae occur at the antipode. Modeling of the Rheasilvia impact predicts significant deformation at and near the impact antipode, however no definite evidence of that amount of deformation at the Rheasilvia antipode are found from the Dawn dataset (Bowling et al., 2014). Blewett et al. (2014) found that the cratered highland near the north pole of Vesta is likely to be a remnant of ancient crust formed before the Rheasilvia impact, and no large-scale troughs were observed there. While several reasons may explain the lack of major antipode structures, such as weakened antipodal constructive interference of seismic waves due to an oblique impact, the non-spherical shape of Vesta, or the physical properties of the interior (Blewett et al., 2014), it remains an open question of how structures as large scale as Divalia Fossae could have formed away from the antipode, yet be directly caused by the impact.

The Divalia Fossae are concentric around the south pole of Vesta and the south pole falls well within the 95% confidence ellipse of the poles to planes through the troughs (Figs. 8 and 9), establishing a geographic correlation with Vesta's spin axis. The asteroid is spinning rapidly with a well-determined rotational period of 5.342 h, and it has a marked equatorial bulge and polar flattening. An origin of the Divalia Fossae related to Vesta's rotation has previously been proposed, including changes in the spin rate of the asteroid and reorientation of the spin axis by the Rheasilvia impact (Schmidt, 2011). These hypotheses suggest the Divalia Fossae were formed by long-term consequences of asteroid tectonics after the Rheasilvia impact, which are permissible with the cross-cutting relationships shown here and previously derived age relationships from crater statistics (Cheng et al., 2021).

In particular, the crater statistics were derived for the Divalia Fossae and compared with those of the Rheasilvia basin to determine their relative age (Cheng et al., 2021). Although the reported crater frequencies permit a simultaneous formation of the two landforms, large uncertainties allow for the Divalia Fossae to have formed well before or after the emplacement of the Rheasilvia basin (Cheng et al., 2021). Since the southernmost trough of the Divalia Fossae cuts the basin-bounding scarp and lies partly within the basin (Figs. 4 and 8), the age of formation of the Divalia Fossae can be constrained to after the Rheasilvia basin was formed.

Crater-counting studies interpreted that the Rheasilvia basin formed at ~0.8 Ga to 3.5 Ga. Crater counting of the entire basin floor (Marchi et al., 2012; Schenk et al., 2012) estimated the basin age to be ~1 Ga and ~1.8 Ga, based on the Main Belt crater production function (O'Brien and Sykes, 2011) and lunar-derived crater production function (Schmedemann et al., 2014), respectively. A different crater counting study (Schmedemann et al., 2014) produced a basin age of ~3.5 Ga. A recently updated crater count and interpretation of Rheasilvia suggests a much younger basin age of ~0.8–0.9 Ga (Schenk et al., 2022). If the Rheasilvia basin is indeed very young, the trough that crosscuts it must be even

¹ <https://www.iau.org/news/announcements/detail/ann14003/>.

younger. However, the Divalia Fossae are heavily degraded (Cheng and Klimczak, 2022), which points against the young age interpretation of the Rheasilvia basin.

Hypotheses that would tie the tectonics of Vesta to long-term consequences of the Rheasilvia impact include the possibility of asteroid reorientation (e.g., Karimi and Dombard, 2016). In particular, the study numerically modeled the potential for relaxation of large south polar basins and a rotational bulge after the asteroid reoriented. The models predict that Vesta's lithosphere was too cold to permit the relaxation of basin topography and the rotational bulge at a time after basin formation, and thus reorientation of Vesta by the Rheasilvia impact was found to be unlikely (Karimi and Dombard, 2016). Alternatively, Mao and McKinnon (2020) suggested an increase in spin rate based on the scale and location of the Rheasilvia impact, which was suggested in this study to have played a role in forming the Divalia and Saturnalia Fossae. The specifics of this scenario for the formation of the Divalia Fossae have yet to be investigated. Our findings challenge the previously proposed origin of the Divalia Fossae, that they were caused directly and immediately by the Rheasilvia impact. Future studies may need to consider alternative hypotheses that satisfy the geographic, cross-cutting, and age relationships we presented here.

6. Conclusions

We have produced a detailed structural map of the Rheasilvia basin to characterize the various structures using rigorous mapping criteria with the aim of quantitatively analyzing the orientations, densities, and cross-cutting relationships of these structures. The basin surface is dominated by scarps near the basin rim and ridges on the basin floor near the central mound. Scarps display a well-preserved clockwise spiral pattern extending from the central mound to basin rim in the eastern part of the basin, with some ridges locally following the same structural trend. This pattern was previously interpreted as modification of the basin by mass-wasting, influenced by the Coriolis effect during the basin modification and collapse. The scarps and ridges lack a clear systematic pattern in the area coinciding with the superposed Veneneia basin, indicating that pre-existing Veneneia structures substantially influenced the orientation of Rheasilvia-associated structures. This indicates that the lithosphere must have been shattered by the Veneneia impact, and that no healing and annealing occurred before the impact that formed the Rheasilvia basin.

The Rheasilvia basin structural map shows that the Divalia Fossae crosscut the basin-bounding scarps, which has not been previously recognized. Likewise, the configuration of the Rheasilvia basin and Divalia Fossae, in contrast to conclusions of previous studies, show no clear geographic correlation. The cross-cutting relationship and configuration of the Rheasilvia basin and Divalia Fossae greatly challenge the widely accepted hypothesis that the Divalia Fossae were formed directly and immediately by the Rheasilvia impact. Taken together with previously established age relationships and the collocation of the poles of troughs with the south pole, the Divalia Fossae are more likely to have formed as a long-term consequence of the Rheasilvia impact tied to changes in rotation of the asteroid, supporting alternative hypotheses of an impact-induced change in spin rate or reorientation of Vesta. The relationships between the Divalia Fossae and Rheasilvia basin established here serve as geologic constraints that must be accounted for when assessing hypotheses that seek to understand the tectonic evolution of Vesta.

CRediT authorship contribution statement

Hiu Ching Jupiter Cheng: Conceptualization, Methodology, Software, Formal analysis, Investigation, Data curation, Writing – original draft, Visualization. **Christian Klimczak:** Conceptualization, Methodology, Writing – review & editing, Supervision.

Declaration of competing interest

The authors declare that they have no known competing financial interests or personal relationships that could have appeared to influence the work reported in this paper.

Acknowledgments

We thank the editor Fabrizio Agosta and two anonymous reviewers very much for their feedback on the earlier version of this paper. We also thank Steven Holland for his discussions on the statistical aspects of this research. The supplemental shapefiles of this manuscript are available at <https://data.mendeley.com/datasets/bxbykxrk7h/1>. We acknowledge and thank the NASA Dawn Mission, instrument teams at the Max Planck Institute, and stereo analysis team at German Aerospace Center (DLR) for the acquisition and processing of Dawn data used in this work. All used Dawn data in this study are archived in the NASA Planetary Data System. The original data used in this study are available from https://pds-smallbodies.astro.umd.edu/data_sb/missions/dawn/index.shtml.

References

- Allmendinger, R.W., Cardozo, N.C., Fisher, D., 2013. *Structural Geology Algorithms: Vectors & Tensors*. Cambridge University Press, Cambridge, England.
- Asphaug, E., 1997. Impact origin of the Vesta family. *Meteoritics Planet Sci.* 32 (6), 965–980. <https://doi.org/10.1111/j.1945-5100.1997.tb01584.x>.
- Asphaug, E., Moore, J.M., Morrison, D., Benz, W., Nolan, M.C., Sullivan, R.J., 1996. Mechanical and geological effects of impact cratering on Ida. *Icarus* 120 (1), 158–184. <https://doi.org/10.1006/icar.1996.0043>.
- Benz, W., Asphaug, E., 1994. Impact simulations with fracture. I. Method and tests. *Icarus* 107 (1), 98–116. <https://doi.org/10.1006/icar.1994.1009>.
- Blewett, D.T., Buczkowski, D.L., Ruesch, O., Scully, J.E., O'Brien, D.P., Gaskell, R., Roatsch, T., Bowling, T.J., Ermakov, A., Hiesinger, H., Williams, D.A., 2014. Vesta's north pole quadrangle Av-1 (Albania): geologic map and the nature of the south polar basin antipodes. *Icarus* 244, 13–22. <https://doi.org/10.1016/j.icarus.2014.03.007>.
- Bowling, T.J., Johnson, B.C., Melosh, H.J., Ivanov, B.A., O'Brien, D.P., Gaskell, R., Marchi, S., 2013. Antipodal terrains created by the Rheasilvia basin forming impact on asteroid 4 Vesta. *J. Geophys. Res.: Planets* 118 (9), 1821–1834. <https://doi.org/10.1002/jgre.20123>.
- Bowling, T.J., Johnson, B.C., Melosh, H.J., 2014. Formation of equatorial graben on 4 Vesta following the Rheasilvia basin forming impact. In: *Vesta in the Light of Dawn: First Exploration of a Protoplanet in the Asteroid Belt*, p. 1773, 2018.
- Buczkowski, D.L., Wyriick, D.Y., Iyer, K.A., Kahn, E.G., Scully, J.E.C., Nathues, A., Gaskell, R.W., Roatsch, T., Preusker, F., Schenck, P.M., Le Corre, L., 2012. Large-scale troughs on Vesta: a signature of planetary tectonics. *Geophys. Res. Lett.* 39 (18) <https://doi.org/10.1029/2012GL052959>.
- Cardozo, N., Allmendinger, R.W., 2013. Spherical projections with OSXStereonet. *Comput. Geosci.* 51, 193–205. <https://doi.org/10.1016/j.cageo.2012.07.021>.
- Cheng, H.C.J., Klimczak, C., 2022. Large-scale troughs on Asteroid 4 Vesta accommodate opening-mode displacement. *J. Geophys. Res.: Planets* 127, e2021JE007130. <https://doi.org/10.1029/2021JE007130>.
- Cheng, H.C.J., Klimczak, C., Fassett, C.I., 2021. Age relationships of large-scale troughs and impact basins on Vesta. *Icarus* 366, 114512. <https://doi.org/10.1016/j.icarus.2021.114512>.
- Collins, G.S., Morgan, J., Barton, P., Christeson, G.L., Gulick, S., Urrutia, J., Warner, M., Wünnemann, K., 2008. Dynamic modeling suggests terrace zone asymmetry in the Chicxulub crater is caused by target heterogeneity. *Earth Planet Sci. Lett.* 270 (3–4), 221–230. <https://doi.org/10.1016/j.epsl.2008.03.032>.
- Drake, M.J., Consolmagno, G.J., 1977. Asteroid 4 Vesta: possible bulk composition deduced from geochemistry of eucrites. In: *Lunar and Planetary Science Conference*, vol. 8.
- Ivanov, B.A., Melosh, H.J., 2013. Two-dimensional numerical modeling of the Rheasilvia impact formation. *J. Geophys. Res.: Planets* 118 (7), 1545–1557. <https://doi.org/10.1002/jgre.20108>.
- Jaumann, R., Williams, D.A., Buczkowski, D.L., Yingst, R.A., Preusker, F., Hiesinger, H., Schmedemann, N., Kneissl, T., Vincent, J.B., Blewett, D.T., Buratti, B.J., 2012. Vesta's shape and morphology. *Science* 336 (6082), 687–690. <https://doi.org/10.1126/science.1219122>.
- Jutzi, M., Asphaug, E., Gillet, P., Barrat, J.A., Benz, W., 2013. The structure of the asteroid 4 Vesta as revealed by models of planet-scale collisions. *Nature* 494 (7436), 207–210. <https://doi.org/10.1038/nature11892>.
- Karimi, S., Dombard, A.J., 2016. On the possibility of viscoelastic deformation of the large south polar craters and true polar wander on the asteroid Vesta. *J. Geophys. Res.: Planets* 121 (9), 1786–1797. <https://doi.org/10.1002/2016JE005064>.
- Kneissl, T., van Gasselt, S., Neukum, G., 2011. Map-projection-independent crater size-frequency determination in GIS environments—new software tool for ArcGIS. *Planet. Space Sci.* 59 (11–12), 1243–1254. <https://doi.org/10.1016/j.pss.2010.03.015>.

- Krohn, K., Jaumann, R., Otto, K., Hoogenboom, T., Wagner, R., Buczkowski, D.L., Garry, B., Williams, D.A., Yingst, R.A., Scully, J., De Sanctis, M.C., 2014. Mass movement on Vesta at steep scarps and crater rims. *Icarus* 244, 120–132. <https://doi.org/10.1016/j.icarus.2014.03.013>.
- Li, J.Y., Mafé, J.N., 2012. Body-fixed Coordinate Systems for Asteroid (4) Vesta. *Planetary Data System*.
- Liu, Z., Yue, Z., Michael, G., Gou, S., Di, K., Sun, S., Liu, J., 2018. A global database and statistical analyses of (4) Vesta craters. *Icarus* 311, 242–257. <https://doi.org/10.1016/j.icarus.2018.04.006>.
- Mao, X., McKinnon, W.B., 2020. Spin evolution of Ceres and Vesta due to impacts. *Meteoritics Planet Sci.* 55 (11), 2493–2518. <https://doi.org/10.1111/maps.13594>.
- Marchi, S., McSween, H.Y., O'Brien, D.P., Schenk, P., De Sanctis, M.C., Gaskell, R., Jaumann, R., Mottola, S., Preusker, F., Raymond, C.A., Roatsch, T., 2012. The violent collisional history of asteroid 4 Vesta. *Science* 336 (6082), 690–694. <https://doi.org/10.1126/science.1218757>.
- Marzari, F., Cellino, A., Davis, D.R., Farinella, P., Zappala, V., Vanzani, V., 1996. Origin and evolution of the Vesta asteroid family. *Astron. Astrophys.* 316, 248–262.
- McCord, T.B., Adams, J.B., Johnson, T.V., 1970. Asteroid Vesta: spectral reflectivity and compositional implications. *Science* 168 (3938), 1445–1447. <https://doi.org/10.1126/science.168.3938.1445>.
- Melosh, H.J., 1989. Impact Cratering: A Geologic Process. Oxford University Press, New York. Oxford: Clarendon Press.
- Melosh, H.J., McKinnon, W.B., 1988. The Tectonics of Mercury. Mercury. University of Arizona Press, pp. 374–400.
- Meschede, M.A., Myhrvold, C.L., Tromp, J., 2011. Antipodal focusing of seismic waves due to large meteorite impacts on Earth. *Geophys. J. Int.* 187 (1), 529–537. <https://doi.org/10.1111/j.1365-246X.2011.05170.x>.
- Murray, B.C., Belton, M.J., Danielson, G.E., Davies, M.E., Gault, D.E., Hapke, B., O'Leary, B., Strom, R.G., Suomi, V., Trask, N., 1974. Mercury's surface: preliminary description and interpretation from Mariner 10 pictures. *Science* 185 (4146), 169–179.
- O'Brien, D.P., Sykes, M.V., 2011. The origin and evolution of the asteroid belt—implications for Vesta and Ceres. *Space Sci. Rev.* 163 (1–4), 41–61. <https://doi.org/10.1007/s11214-011-9808-6>.
- Otto, K.A., Jaumann, R., Krohn, K., Matz, K.D., Preusker, F., Roatsch, T., Schenk, P., Scholten, F., Stephan, K., Raymond, C.A., Russell, C.T., 2013. Mass-wasting features and processes in Vesta's south polar basin Rheasilvia. *J. Geophys. Res.: Planets* 118 (11), 2279–2294. <https://doi.org/10.1002/2013JE004333>.
- Otto, K.A., Jaumann, R., Krohn, K., Spahn, F., Raymond, C.A., Russell, C.T., 2016. The Coriolis effect on mass wasting during the Rheasilvia impact on asteroid Vesta. *Geophys. Res. Lett.* 43 (24), 12–340. <https://doi.org/10.1002/2016GL071539>.
- Pieters, C.M., Ammannito, E., Blewett, D.T., Denevi, B.W., De Sanctis, M.C., Gaffey, M.J., Le Corre, L., Li, J.Y., Marchi, S., McCord, T.B., McFadden, L.A., 2012. Distinctive space weathering on Vesta from regolith mixing processes. *Nature* 491 (7422), 79–82. <https://doi.org/10.1038/nature11534>.
- Poelchau, M.H., Kenkmann, T., 2008. Asymmetric signatures in simple craters as an indicator for an oblique impact direction. *Meteoritics Planet Sci.* 43 (12), 2059–2072. <https://doi.org/10.1111/j.1945-5100.2008.tb00661.x>.
- Preusker, F., Scholten, F., Matz, K.D., Roatsch, T., Jaumann, R., Raymond, C.A., Russell, C.T., 2016. DAWN FC2 DERIVED VESTA DTM SPG V1.0, DAWN-A-FC2-5-VESTADTMSPG-V1.0, NASA Planetary Data System.
- Roatsch, T., Kersten, E., Matz, K.D., Preusker, F., Scholten, F., Elgner, S., Schroeder, S.E., Jaumann, R., Raymond, C.A., Russell, C.T., 2015. Dawn FC2 Derived Vesta Global Mosaics V1. 0. NASA Planetary Data System, DAWN-A.
- Russell, C.T., Raymond, C.A., 2011. The Dawn mission to Vesta and Ceres. In: Russell, C., Raymond, C. (Eds.), The Dawn Mission to Minor Planets 4 Vesta and 1 Ceres. Springer, New York, NY, pp. 3–23. https://doi.org/10.1007/978-1-4614-4903-4_2.
- Russell, C.T., Raymond, C.A., Coradini, A., McSween, H.Y., Zuber, M.T., Nathues, A., De Sanctis, M.C., Jaumann, R., Konopliv, A.S., Preusker, F., Asmar, S.W., 2012. Dawn at Vesta: testing the protoplanetary paradigm. *Science* 336 (6082), 684–686. <https://doi.org/10.1126/science.1219381>.
- Schäfer, M., Nathues, A., Williams, D.A., Mittlefehldt, D.W., Le Corre, L., Buczkowski, D. L., Kneissl, T., Thangjam, G.S., Hoffmann, M., Schmedemann, N., Schäfer, T., 2014. Imprint of the Rheasilvia impact on Vesta—geologic mapping of quadrangles Gegania and Lucaria. *Icarus* 244, 60–73. <https://doi.org/10.1016/j.icarus.2014.06.026>.
- Schenk, P.M., Neesemann, A., Marchi, S., Otto, K., Hoogenboom, T., O'Brien, D.P., Castillo-Rogez, J., Raymond, C.A., Russell, C.T., 2022. A young age of formation of Rheasilvia basin on Vesta from floor deformation patterns and crater counts. *Meteoritics Planet Sci.* 57 (1), 22–47. <https://doi.org/10.1111/maps.13772>.
- Schenk, P., Vincent, J.B., O'Brien, D.P., Jaumann, R., Williams, D., 2012. Impact crater morphologies on Vesta. *September Eur. Planet. Sci. Congr.* 7, 700.
- Schmidt, B.E., 2011. Tectonics of Vesta: indication of spin-up and reorientation? December. In: AGU Fall Meeting Abstracts, vol. 2011. U21B-06.
- Schultz, P.H., Crawford, D.A., 2011. Origin of Nearside Structural and Geochemical Anomalies on the Moon, vol. 477. Geological Society of America Special Papers, pp. 141–159.
- Schultz, P.H., Gault, D.E., 1975. Seismic effects from major basin formations on the Moon and Mercury. *Moon* 12 (2), 159–177. <https://doi.org/10.1007/BF00577875>.
- Scully, J.E., Yin, A., Russell, C.T., Buczkowski, D.L., Williams, D.A., Blewett, D.T., Ruesch, O., Hiesinger, H., Le Corre, L., Mercer, C., Yingst, R.A., 2014. Geomorphology and structural geology of Saturnalia Fossae and adjacent structures in the northern hemisphere of Vesta. *Icarus* 244, 23–40. <https://doi.org/10.1016/j.icarus.2014.01.013>.
- Sierks, H., Keller, H.U., Jaumann, R., Michalik, H., Behnke, T., Bubenhanen, F., Brüttner, I., Carsenty, U., Christensen, U., Enge, R., Fiethe, B., 2011. The Dawn framing camera. *Space Sci. Rev.* 163 (1–4), 263–327. <https://doi.org/10.1007/s11214-011-9745-4>.
- Stein, S., Wyssession, M., 2009. An Introduction to Seismology, Earthquakes, and Earth Structure. John Wiley & Sons.
- Stickle, A.M., Schultz, P.H., Crawford, D.A., 2015. Subsurface failure in spherical bodies: a formation scenario for linear troughs on Vesta's surface. *Icarus* 247, 18–34. <https://doi.org/10.1016/j.icarus.2014.10.002>.
- Thomas, P.C., Binzel, R.P., Gaffey, M.J., Zellner, B.H., Storrs, A.D., Wells, E., 1997. Vesta: spin pole, size, and shape from HST images. *Icarus* 128 (1), 88–94. <https://doi.org/10.1006/icar.1997.5736>.
- The IAU WG Cartographic Coordinates & Rotational Elements (WGCRE), 2014. New Coordinate System for (4) Vesta.
- Williams, D.A., Greeley, R., 1994. Assessment of antipodal-impact terrains on Mars. *Icarus* 110 (2), 196–202. <https://doi.org/10.1006/icar.1994.1116>.
- Williams, D.A., Jaumann, R., McSween Jr., H.Y., Marchi, S., Schmedemann, N., Raymond, C.A., Russell, C.T., 2014. The chronostratigraphy of protoplanet Vesta. *Icarus* 244, 158–165. <https://doi.org/10.1016/j.icarus.2014.06.027>.
- Wilson, L., Head, J.W., 2015. Groove formation on Phobos: testing the Stickney ejecta emplacement model for a subset of the groove population. *Planet. Space Sci.* 105, 26–42. <https://doi.org/10.1016/j.pss.2014.11.001>.
- Yingst, R.A., Mest, S.C., Berman, D.C., Garry, W.B., Williams, D.A., Buczkowski, D., Jaumann, R., Pieters, C.M., De Sanctis, M.C., Frigeri, A.L., Le Corre, L., 2014. Geologic mapping of Vesta. *Planet. Space Sci.* 103, 2–23. <https://doi.org/10.1016/j.pss.2013.12.014>.